Article

Construction and Experimental Study of a 3-Dof Haptic Master for Interactive Operation

Huijun Li *, Aiguo Song, Baoguo Xu, Bowei Li, Hong Zeng and Zhen Lin

School of Instrument Science and Engineering, Southeast University, Nanjing 210096, China; lihuijun@seu.edu.cn

* Correspondence: lihuijun@seu.edu.cn; Tel.: +86-025-8379-3293

Abstract: This paper presents a novel 3-degrees-of-freedom (3-DOF) haptic master with rubber bands for self-resetting. The mechanical design avoids coupling between three directions mechanically by using three perpendicular axis intersecting at one point. Bevel gear transmission is adopted to increase the compactness of the overall structure. VR-based interactive system is designed and built by incorporating the proposed haptic master. The proposed haptic device can generate force feedback along 3-degree-of-freedom motion using motors and provide command signals to the avatar in the virtual environment. In order to analyze the performance of the developed device in terms of haptic feedback operation, ergonomics assessments are designed and experimentally implemented. Preliminary studies on the influencing factor including the guidance force, the reset force, the speed of the avatar and the arm the length have been conducted. The results of this paper are of great significance for the design of the haptic master and interactive system.

Keywords: haptic master; force feedback; VR-based interaction; ergonomics assessments

1. Introduction

The development of many applications of interactive operation requires flexible haptic master to perform contact tasks. These tasks include interaction with computer aided design models, flight simulators, telerobotic surgery, micro/nano-manipulation, undersea salvage, as well as telerobotic maintenance and decontamination and decommissioning of chemical and nuclear facilities [1,2].

The execution of these tasks by an operator is affected by his/her level of perception of the interaction [3]. This illusion of presence is enhanced by audio, visual and haptic cues. While visual cues are certainly mandatory, and audio cues beneficial at times, haptic cues can significantly improve the flow of information from the environment to the operator for many tasks requiring dexterity [4]. Several types of haptic master devices featuring the feedback function have been proposed, some of which are commercially available devices and some are experimental prototypes [5-7]. The PHANToM, which is the most commonly used haptic device, can generate force feedback along 6-degree-of-freedom (DOF) motions using motors [8]. The Xitack IHP of Xitack SA, which has been proposed for virtual reality applications, has 4-DOF force feedback functions [9]. Dual ArmWork Platform (DAWP) at Argonne National Laboratory [10], one of the key improvements the Cobotic Hand Controller can provide to DAWP operation is the implementation of virtual surfaces, or virtual constraints on motion, as suggested by Faulring [11]. Such master devices can reproduce the constraints or guidance of the slave site and can vastly simplify execution of a contact task. While guidance or constraints can be implemented at the slave side in the existing system, an active master allows for the reproduction of these guidance or constraints at the master and may reduce operator fatigue while increasing efficiency by eliminating unneeded or wrong motions in workspace. Thus,

 doi:10.20944/preprints201712.0012.v1

if the operator is inserting a peg into a hole and constrains the motion of the peg to the plane of the objects at the slave but guides it to the top of the hole, he/she feels these same constraints and guidance at the master.

There are mainly three kinds of haptic masters. CyberGrasp is typical force feedback gloves which are in form of external skeleton and can make people feel the interactive force by exerting forces on the fingertips according to the degree of stretch of the joints of the fingers [12]. The arm force feedback device can provide force feedback to the operators at multiple degrees of freedom. Such devices have large load structures, with multiple degrees of freedom, allowing complex movement. The typical device of this kind is Omni produced by Sensable Technologies. The body force feedback devices are generally large and complex that not only support the movement of the upper limbs, but also provide a wide range of movements of the lower limbs including the hip, knee and ankle joints, so the device is generally in the form of the outer skeleton. The typical device of this kind is Haptic Walker [13].

Current trend in mechanical design of haptic masters is to meet the need for designs with safety, high performance, sufficient workspace, enough force and torque, high stiffness, and small inertia [14-16]. By their nature, haptic masters operate in contact with a human operator. Greater research effort on the operator's perception and overall performance using the haptic masters could accelerate the development of haptic interaction technology [17-19]. In these research, the haptic perception of the users was optimized and evaluated using haptic devices. Human factors as well as others that affect the design specifications of force-reflecting haptic interfaces were also concerned [20].

Although a number of commercial and research haptic masters are becoming available, their applications have been limited. Large improvements on existing devices can only be achieved by a proper match between the performance of the device and human haptic abilities. The hope that the generating synthesized haptic experiences is adequate for a particular task. To find out how the users can complete the operation with a haptic master by creating synthetic haptic experiences, quantitative human studies are essential. To determine the nature of these approximations, or, in other words, to find out what we can get away with in creating synthetic haptic experiences, ergonomics studies are essential. Understanding of such influencing factors as the guidance force, the reset force, the speed of the virtual avatar and the arm length is critical for proper design specification of the hardware and software of haptic interfaces.

In this paper we introduced a novel 3-degrees-of-freedom (3-DOF) haptic device with self –resetting rubber bands and concerned with quantitative measures of influencing factors that affect the overall performance and then the design specifications of force-reflecting haptic master. The remainder of the paper is organized as follows. Mechanical design and kinematical analysis is presented in Section 2. VR-based interactive system is analyzed in Section 3. Experimental setting is presented in Section 4, and the performance of the proposed system is verified experimentally in Section 5. The paper is then concluded in Section 6.

2. Three-DOF Haptic Master

2.1. Mechanical Design

Mechanical design of haptic masters is to meet the need for designs with sufficient workspace, enough force and torque, high stiffness, small inertia and mechanical singularity. However, some of these requirements, such as large stiffness and small inertia, are conflicting in nature [21, 22]. Due to the multi-criteria and multi-domain functional and performance requirements of high-performing haptic devices, it is not sufficient to develop such a device by sub-optimizing the requirements from each separate discipline. The main design objectives of our device are to obtain a large workspace and mechanical singularity, and, at the same time, provide torque feedback along three motion directions. In this paper, a parallel haptic master for interactive operation is designed consisted of three mutually orthogonal translational axes, which has lower inertia and the better stiffness. At the same time, through reasonable layout, the workspace of the handle is increased. The general

Preprints (www.preprints.org) | NOT PEER-REVIEWED | Posted: 3 December 2017 doi:10.20944/preprints201712.0012.v1

assembly drawing of this device is presented in Figures 1. Maxon DC motors for each axis are mounted to provide force feedback. The device is capable of rendering continuous forces up to 25N in X and Y axis and torque of 0.5Nm in Z axis. The user grasps a handle mounted on the end effector which is replaceable.

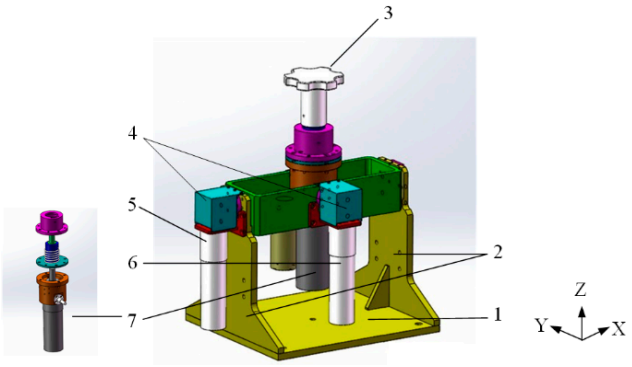

Figure 1. General assembly drawing of the haptic master (1) Base; (2) Cuboid frame; (3) Handle; (4) Bevel gears; (5) (6) Actuators and photoelectric encoders; (7) Cylinder sleeve

The proposed structure is similar to a 3-axis gyroscope in which three axes are orthogonal and intersect at a fixed point that will not change its position while the handle moves or rotates. At the same time, each kinematic singularity is independent and there is no movement intervention which means that coupling is avoided.

The device mainly consists of the base, the cuboid frame and cylindrical sleeve, three actuators and photoelectric encoders, a torsion spring for restoration of rotation in Z axis, two rubber bands for self-resetting in X and Y axis, the handle and couplings. The cuboid frame and the cylindrical sleeve are moved in X- and Y-direction through the shaft, and the operating handle is rotated around Z axis by the rotary shaft.

to measure the rotation angle in three degrees of freedom

Three Maxon encoders are utilized to measure the rotation angles in three degrees of freedom around the motor shafts that are used to calculate the pose of the operating handle, which is coherent with the motion of the operator. Three DC motors manufactured by Maxon Corporation are used to generate the force / torque feedback along X, Y, and Z axis respectively to act on the operator's hand. The forces feedback generated by the actuators on X and Y axis are transferred by two bevel gears to ensure the consistent directions with X and Y axis. While haptic devices usually work a low speed and provide high torque, corresponding reducer are equipped to increase the motor output torque and to reduce the rotational speed. In addition, restoration mechanism is designed to make the haptic device return to the originating pose after operating. In the cylindrical sleeve a torsion spring is installed for rotation restoration around Z axis by placing each end in the position limitation holes which are connected to the actuator and to the handle respectively. While the handle rotates around Z axis, the torsion spring elastic force acts as restoration force. Each end of two rubber bands is fixed at the bottom of the middle actuators and the frame respectively, pulling to each side to realize zero reset in X and Y axis by the elastic forces of the rubber bands. Also buttons are equipped at the end of the handle to implement restoration during movement and to switch the functional mode. Such mechanism design is valuable for high stiffness, small inertia and mechanical singularity and other aspects. The developed haptic device is shown in Figure 2.

Preprints (www.preprints.org) | NOT PEER-REVIEWED | Posted: 3 December 2017 doi:10.20944/preprints201712.0012.v1

Figure 2. Prototype of the designed 3-DOF haptic master

2.2. Kinematics analysis

The Kinematic diagram of the designed haptic master is described in Figure 3. The motion of the haptic device to any point in the workspace can be decomposed into motion components on x-o-z plane and y-o-z plane respectively.

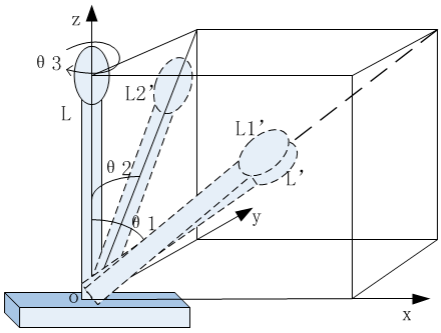

Figure 3. Kinematical Diagram of the Designed Haptic Master

Assuming that the length of the handle bar is l and the rotational angles of on x-o-z plane and y-o-z plane are θ1 and θ2 respectively, if the coordinates of the end of the handle are (Px, Py, Pz), the relationship between the position of the end, the rotational angles of the handle and the length of the handle bar l is (ignoring minor deformation of the bar),

$$P_x = \frac{l \times tan\theta_1}{\sqrt{1+(tan\theta_1)^2+(tan\theta_2)^2}} \quad (1)$$

$$P_y = \frac{l \times tan\theta_2}{\sqrt{1+(tan\theta_1)^2+(tan\theta_2)^2}} \quad (2)$$

$$P_z = \frac{l}{\sqrt{1+(tan\theta_1)^2+(tan\theta_2)^2}} \quad (3)$$

The rotational ranges of the haptic device along X, Y, Z are -60°~60°，-60°~60°，-90°~90° respectively and the distance from the center of rotation to the end of the handle is 150 mm, so the motion space of the haptic master can be deduced to be a spherical surface from formula (1-3) and its workspace is up to 259.72mm * 259.72mm * 93.30mm, as is drawn in Matlab as Figure 4.

Preprints (www.preprints.org) | NOT PEER-REVIEWED | Posted: 3 December 2017 doi:10.20944/preprints201712.0012.v1

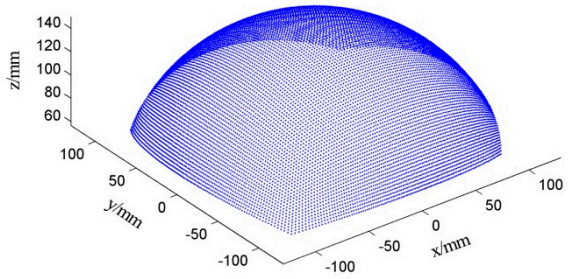

Figure 4. Working space of the developed haptic master

3. VR-Based Force Feedback Interactive System

3.1. System Construction

VR-based system consists of the operator, the haptic master, the virtual environment which integrates with the geometric model, the kinematic model, the controller and the force rendering module. Figure 5 shows the schematic diagram of the system. In such a system, the haptic master is utilized to acquire the motion of the operator's hand and to provide force feedback so that the operator can control the avatar in VR and feel the interactive force between the avatar and the virtual objects. The virtual environment is used to create a digital model of the physical world in the computer and calculate the virtual force according to different operations based on operational kinematics and dynamics of different tasks. The goal of force rendering is to convert the calculated virtual forces to match the capabilities of the virtual force signal with the force-sensing interaction device to ensure stable force feedback. When a human operator operates the haptic master, command (x_m) is sent out to the virtual environment to control the avatar and virtual force (f_v) is fed back to the operator with graphical refresh at the same time.

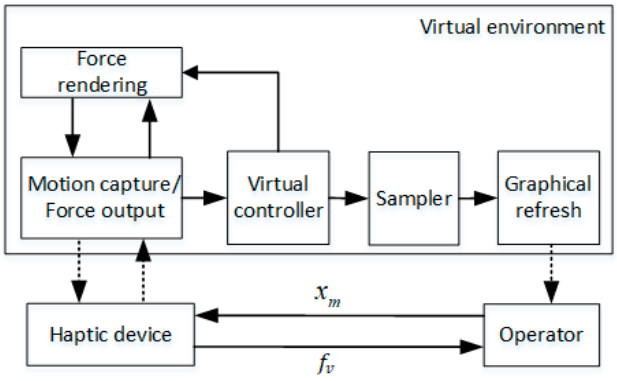

Figure 5. The structure diagram of the VR-based haptic interactive system

One of the major goals in this system is to provide the operator with force and visual feedback. The graphic model maintains the information about the current geometric states of the avatar and the environment. Collision detection is conducted while performing tasks in the virtual environment. This allows the virtual objects to deform and give counterforce to the avatar. This force generated in the virtual environment exerts on the operator at the same time. Then the operator holding the haptic master feels the counterforce acting on the avatar and watches the motion of the virtual objects on the screen. The combination of visual and force feedback makes the operator feel the interaction of the virtual environment.

Preprints (www.preprints.org) | NOT PEER-REVIEWED | Posted: 3 December 2017 doi:10.20944/preprints201712.0012.v1

In order to improve the frequency of force feedback, the virtual environment module is divided into two loops, one is for visual display and the other is for force feedback. Since the two loops can be processed independently, the virtual force can be rendered at a high frequency of 500~1KHz to ensure the continuity and stable perception for the operator. The graphics update loop is to complete the collision detection, the collision response (including deformation calculation and graphics rendering) at a lower frequency of tens of hertz.

3.2. Software Design

The system software provides interface display and visual feedback for the operator. The whole software is developed in Microsoft Visual Studio2008 platform, based on MFC framework and Measurement Studio. OpenGL is used as a graphical interface to render the 3D virtual scene and to complete the dynamic elements loading. The overall flowchart of the software is shown in Figure 6.

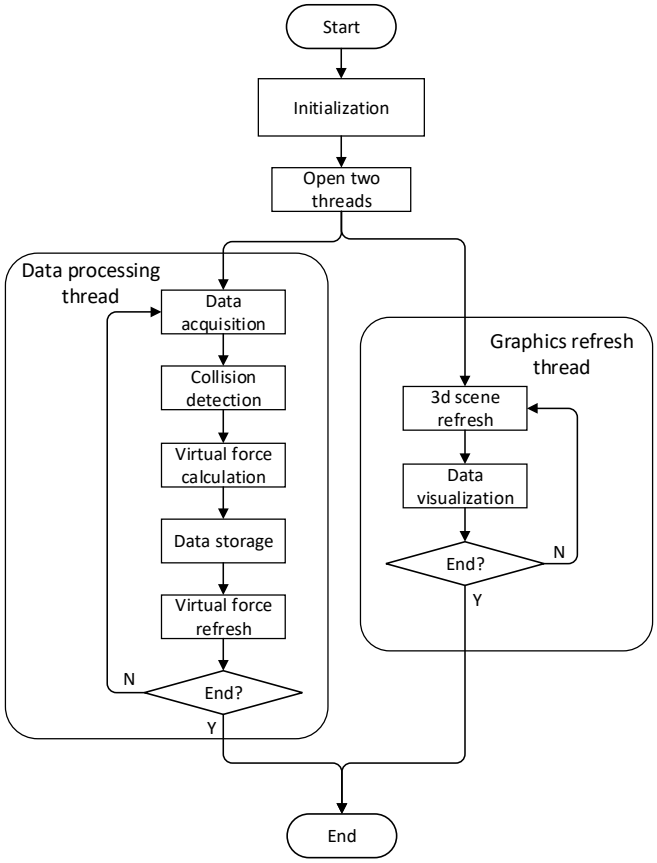

Figure 6. Flow chart of the haptic feedback environment

According to the function of each module of the force feedback system, the layout of the whole software is designed in detail. There are several different functional areas in the software interface. The first is serial mode setting area. Serial communication mode is mainly uses in this system. Before opening the serial port, the operator need to set the serial port parameters by pulling down the menu on the serial port baud rate, serial number to choose to improve the software versatility and compatibility. The Operators can also open or turn off the serial port at any time and reset the entire software. The second is data storage area which includes the degree of information on each degree of freedom, the location and speed of the virtual avatar, and the feedback force information of each degree of freedom. In the experimental operation, the operator can click the Save button to save the data in the specified path in a certain format to save as a text document. The third is data visualization area. In order to understand the angle information and feedback force information in real-time intuitively, the operator can click the monitor button to pop up a new window to display

Preprints (www.preprints.org) | NOT PEER-REVIEWED | Posted: 3 December 2017 doi:10.20944/preprints201712.0012.v1

the three degrees of freedom and virtual force feedback in dials and waveforms. The fourth is virtual scene selection area. In order to adapt to different operating environment and experimental tasks, three different virtual environments are designed in the software, namely the flexible ball scene model, virtual robotic task scene and ball tracking scene. The operator can switch according to their own needs to operate in the corresponding scenario. The last is operation mode selection area. The haptic master is designed in line with the principles of ergonomic to adapt to the human body arm operating habits and with a suitable elastic reset force to ensure self-resetting. Because the haptic master is similar to the selector or joystick, it can be used for position control or speed control. The operator can quickly switch between the position control mode and the speed control mode in this area. The overall software interface is shown in Figure 7.

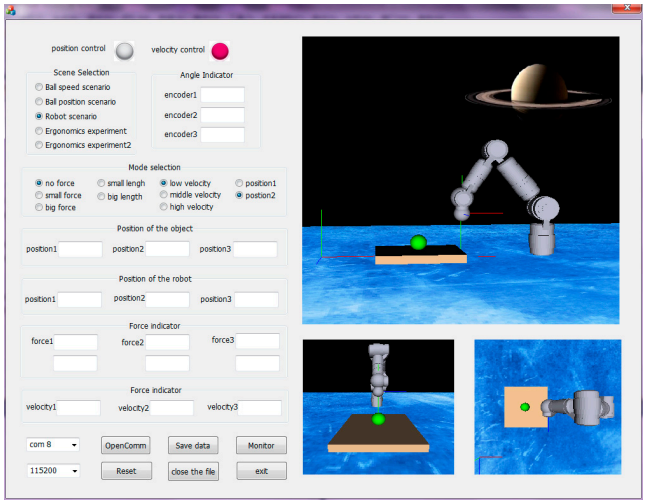

Figure 7. Software Interface of the Force Feedback System

3.3. Virtual Force Feedback

In the VR-based system, coordinated visual and force feedback can improve the perception of the operator. Generally, the God-Object algorithm can be used to calculate the interactive force between the avatar and the virtual object. According to the single point contact linear dynamic model, when the avatar interacts with the virtual object, the virtual force is,

$$f_v = \begin{cases} 0 & x_v < x_e \\ k_v(x_v - x_e) & x_v \geq x_e \end{cases} \quad (4)$$

wherein f_v denotes the interaction force between the avatar and the virtual object, x_v and x_e represent the location of the contact point and the virtual agent point respectively, k_v is the virtual wall stiffness. The feedback force is limited by setting the maximum threshold in the software so that it will not exceed the allowable force range.

4. Experiments

4.1. Experimental System

The haptic master is mainly used in the field of VR-based interaction and teleoperation to acquire the movement of the operator's hand and to provide the operator with force feedback. As man-machine interactive interface, not only mechanical but also ergonomic characters are important. In order to experimentally evaluate the performance of the developed haptic master, we built a prototype of VR-based interactive system for experiments. Several ergonomic experiments are designed and performed. Effective data collected is utilized to statistically analyze the characteristics and efficiency while using the developed haptic master.

The experimental system consists of the developed haptic master, the virtual environment and the operator, as shown in Figure 8. The operator can control the avatar and sense the force feedback

Preprints (www.preprints.org) | NOT PEER-REVIEWED | Posted: 3 December 2017 doi:10.20944/preprints201712.0012.v1

of the virtual environment, such as contact force, frictional force, guidance force, etc., through the haptic master.

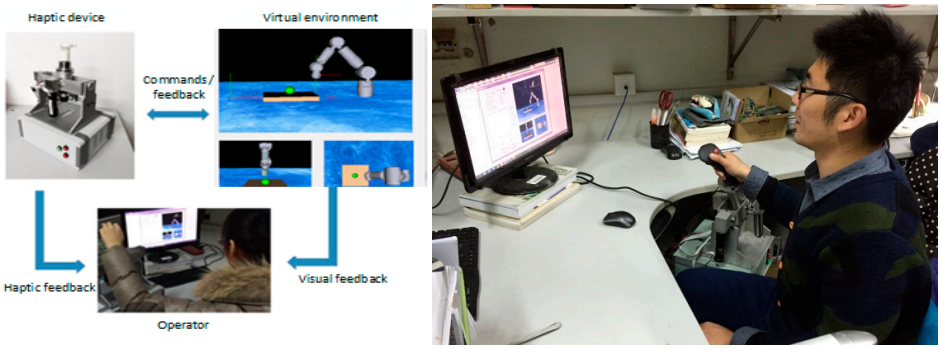

Figure 8. Experimental system

4.2. Experimental Tasks

In this study, we mainly analyze several factors that play a significant role in the haptic interactive system, including the guidance force, the reset force, the speed of the avatar and the arm length. Ten healthy volunteers aged 20-30 years (habitual use of the right hand) participated in the experiments. The experiments consist of two parts. The first part is the virtual robotic task scenario shown as Figure 9(a). In this task scenario, the operator should control the virtual arm through the haptic device to grasp the green ball on the yellow plane, then move it to the red ball and release. Catching or releasing the ball is switched by the button on the handle of the haptic master. In this experiment, no guidance is provided and the operator should plan their own path according to the information available to them. The second part of the experiment is ball tracking scenario shown in Figure 9 (b). This is a path-guided operational task. The operator should control the blue ball through the haptic master to track the pink ball following the preset path. Once the blue ball touched the pink ball, the latter moved to the next positon and the operator should go on tracking. The entire process consists of six such cycles.

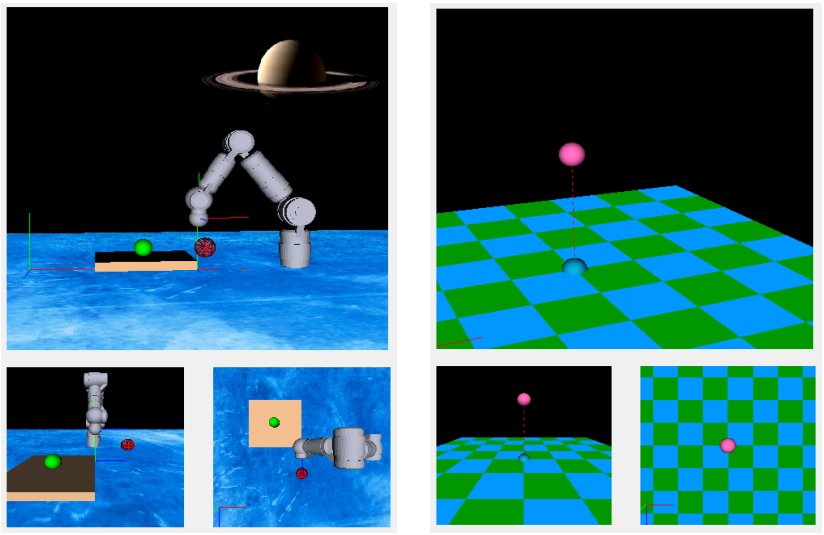

(a) (b)

Figure 9. Experimental Tasks. (a) Virtual robotic scenario; (b) Ball tracking scenario

Variable-controlling approach is applied in the experiment to analyze the effects of each factor on the interactive operation. The first factor is the guidance force (f_g) provided by the haptic master to guide the operator move to the target. Suppose the guidance force of 0N, 2N, 4N is for condition

Preprints (www.preprints.org) | NOT PEER-REVIEWED | Posted: 3 December 2017 doi:10.20944/preprints201712.0012.v1

a1, a2 and a3 respectively. The second factor is the reset force (f_r) which drivers the haptic device back to the initial pose. Suppose the reset force of 0N, 2N, 4N is for condition b1, b2 and b3 respectively. The third is the speed of the virtual avatar which is set at 0.5cm/s, 1.5cm/s and 2.5cm/s for the condition c1, c2 and c3 respectively.

Among all the control factors, a1, b1, c2 are the default control factors. During the experiments, when the influence of a variable is studied, the control factor of this variable is changed, and other variables are the default factors. For example, three groups of experiments at condition a1*b1*c2、a2*b1*c2、a3*b1*c2 should be carried out to study the effect of the guidance force in the virtual robotic scenario and the ball tracking scenario respectively. So each subject needs to do 18 experiments and the experimental sequences of each subject were randomly arranged.

5. Results and Analysis

5.1. Effects of the Guidance Force

Three levels of 0N, 2N, and 4N were applied in the experiment to investigate the influence of the guidance force on the operation efficiency of the haptic interactive system. The elapsed time for completing the designed task was recorded, as is shown in Table 1.

Table 1. Average Task Completion Time (Second)

Subjects	Virtual robotic scenario			Ball tracking scenario		
	f_g=0N	f_g =2N	f_g =4N	f_g =0N	f_g =2N	f_g =4N
1	21.625	18.633	17.846	46.157	40.492	38.491
2	25.648	24.765	22.694	53.719	48.468	46.189
3	16.654	14.369	15.432	66.492	62.483	55.371
4	18.462	16.751	16.345	49.755	44.392	43.034
5	25.349	21.459	21.469	62.449	58.428	55.482
6	28.394	28.200	25.624	55.664	52.983	52.648
7	23.462	21.954	18.694	53.469	52.694	48.691
8	23.489	20.645	19.369	49.648	44.669	45.893
9	19.762	19.239	17.425	51.673	50.945	50.694
10	21.694	20.469	20.964	55.644	52.469	50.442

According to the statistical data in Table 1, task completion time histogram of each operator with three levels of guidance force in two scenarios is shown in Figure 10.

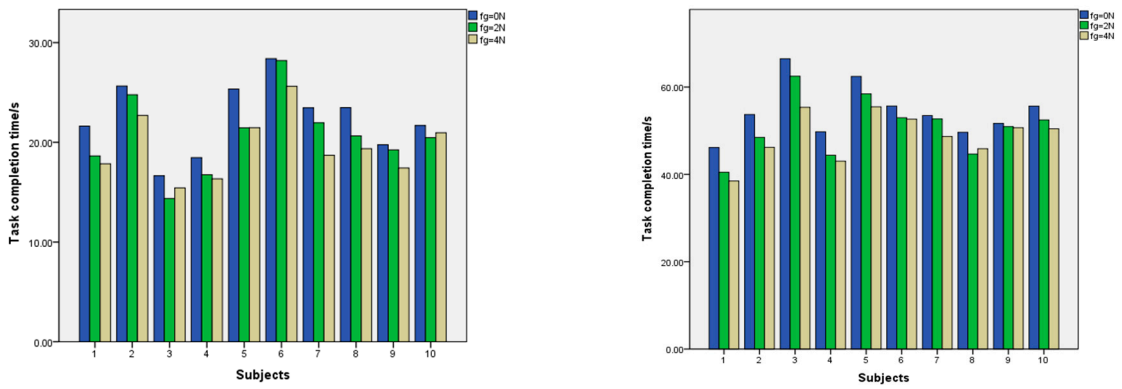

Figure 10. Task completion time histogram in two different scenarios. (a) Virtual robotic scenario; (b) Ball tracking scenario.

Preprints (www.preprints.org) | NOT PEER-REVIEWED | Posted: 3 December 2017 doi:10.20944/preprints201712.0012.v1

As can be seen from the Figure 10, the overall distribution of task completion time in three cases is consistent although the task completion time of ten subjects is slightly different. The guidance force will shorten the task completion time in both two scenarios. In the case of the virtual robot scenario, task completion time was reduced by 15.3% at most and 8% on average with 2N guidance force compared with no guidance force. When 4N guidance force was available, task completion time was shortened by 20.3% at most and 12.7% on average compared with no guidance force. In the ball tracking scenario, task completion time reduction was 10.77% at most and 6.7% on average with 2N guidance force compared with no guidance force. When 4N guide force was available, task completion time was shortened by 16.60% at most and 10.6% on average. The result indicates that the guidance force can give the operator a certain operation hint which can help to improve the operation efficiency and to shorten the task completion time. Although task completion time is averagely shortened with 4N guide force compared with 2N guide force, further experiments should be carried out to study the optimal guidance force for different subjects and different tasks.

5.2. Relationship between the Reset Force and the Operating Range

To study the effect of the reset force on the interactive operation, the reset force was set at three grades that include elastic force of the rubber bands only, elastic force plus 2N motor output and elastic force plus 4N motor output. Other variables were the default factor. Univariate analysis of variance was used to analyze. Table 2 shows the result of variance analysis of the maximum operating angle (in degree) in six motion directions.

Table 2. Analysis of variance the maximum operating angle in six movement directions

		Sum of the squares	df	Mean square	F	Significance
X+ (°)	inter-group	279.912	2	139.956	4.651	0.018
	intra-group	812.525	27	30.094		
	Sum	1092.437	29			
X- (°)	inter-group	526.287	2	263.144	6.465	0.005
	intra-group	1099.021	27	40.704		
	Sum	1625.308	29			
Y+ (°)	inter-group	473.750	2	236.875	10.219	0.000
	intra-group	625.872	27	23.180		
	Sum	1099.622	29			
Y- (°)	inter-group	836.978	2	418.489	5.376	0.011
	intra-group	2101.904	27	77.848		
	Sum	2938.882	29			
Z+ (°)	inter-group	1769.057	2	884.528	6.194	0.006
	intra-group	3855.782	27	142.807		
	Sum	5624.839	29			
Z- (°)	inter-group	1160.788	2	580.394	2.300	0.120
	intra-group	6814.036	27	252.372		
	Sum	7974.824	29			

X+ means the positive direction of X axis X- means the negative direction of X axis. The rest in the same way.

In the result of the variance analysis given in Table 2, the sum of the squared variance, the mean square, the F value and the probability P of the groups are given. From the significance level $P < 0.05$, there was a significant difference in the mean value between groups in the positive and negative directions of the X, Y axis and the positive direction of the Z -axis at 0.05 level.

Preprints (www.preprints.org) | NOT PEER-REVIEWED | Posted: 3 December 2017 doi:10.20944/preprints201712.0012.v1

Figure 11 shows the histogram of the range of the movement of the hand in the positive and negative directions of the X, Y, Z under the conditions of three grades of resetting force. The abscissa in Figure 11 is 1, 2, 3, representing the motor reset force of 0N, 2N and 4N respectively and the vertical axis represents the maximum angle of the operating movement in this direction degree (°).

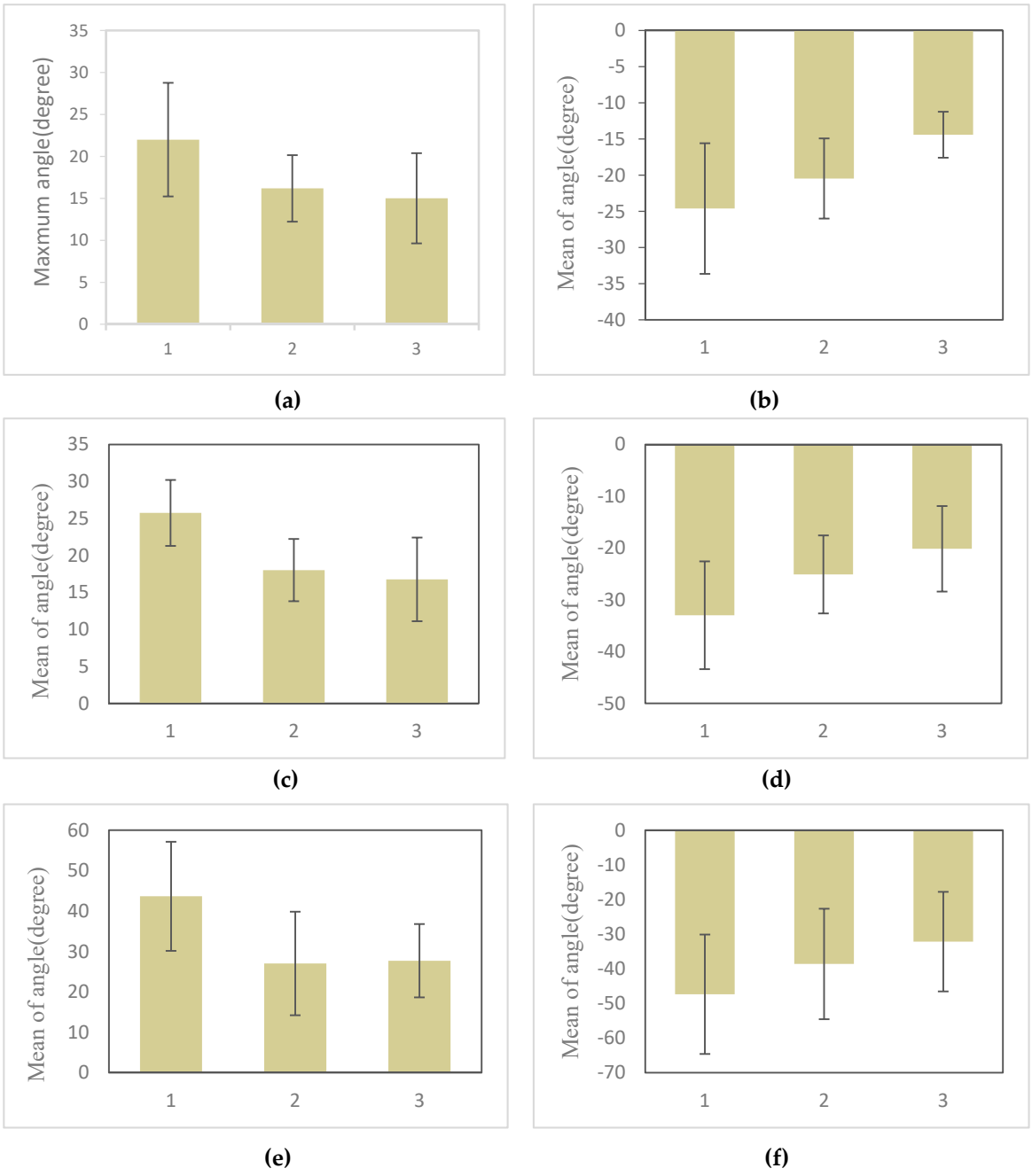

Figure 11. Bar charts of the range of motion with three grades of resetting force (95% CI). (a) In the X axis positive direction; (b) In the X axis negative direction; (c) In the Y axis positive direction; (d)In the Y axis negative direction; (e)In the Z axis positive direction; (f)In the Z axis negative direction.

As can be seen from the Figure 11, the reset force effects the operating range of the haptic master in all motion directions. The greater the reset force, the corresponding operating range is smaller. This is possibly because the reset force constraints the free motion of the operator to some extent. So the reset force should be minimized in the condition that the restoration is ensured.

Preprints (www.preprints.org) | NOT PEER-REVIEWED | Posted: 3 December 2017 doi:10.20944/preprints201712.0012.v1

5.3. Relationship between the Speed of the Avatar and the Operating Range

In this experiment, the speed of the virtual object is set at 0.5m/s, 1.5m/s, 2.5m/s respectively and the other factors are set as default factors. Three groups of the operable range were recorded in degree (°) and one-way analysis of variance (ANOVA) was used to study the effects of different conditions on the experiments. The results are shown in Table 3.

Table 3. Variance Analysis of Virtual Object Motion

		Sum of the squares	df	Mean square	F	Significance
X+ (°)	inter-group	199.247	2	99.624	4.004	0.030
	intra-group	671.833	27	24.883		
	Sum	871.080	29			
X- (°)	inter-group	250.083	2	125.041	2.350	0.115
	intra-group	1436.942	27	53.220		
	Sum	1687.025	29			
Y+ (°)	inter-group	124.523	2	62.261	2.013	0.153
	intra-group	835.071	27	30.929		
	Sum	959.593	29			
Y- (°)	inter-group	354.916	2	177.458	2.142	0.137
	intra-group	2236.635	27	82.838		
	Sum	2591.551	29			
Z+ (°)	inter-group	1412.462	2	706.231	4.761	0.017
	intra-group	4005.187	27	148.340		
	Sum	5417.648	29			
Z- (°)	inter-group	1083.262	2	541.631	1.721	0.198
	intra-group	8496.079	27	314.670		
	Sum	9579.341	29			

It can be seen from the significance level (P) that the intra-group means along X-axis positive direction and Z-axis positive direction are significantly different ($P< 0.05$) while the differences in other directions are not significant. Furthermore, the differences of the measurement data were compared with the homogeneity test of variances and the results indicated there was no significant difference between the variance of each group at 0.05 level, that is, the variance is homogeneous, as is shown in Table 4.

Table 4. Homogeneous test of variance under conditions of different avatar speed

	Levene statistic(°)	**df1**	**df2**	**significance**
X+	1.019	2	27	0.375
X-	1.806	2	27	0.184
Y+	0.985	2	27	0.386
Y-	2.259	2	27	0.124
Z+	0.495	2	27	0.615
Z-	0.371	2	27	0.694

LSD multiple comparison procedure was used for further analysis. In Table 5, the experimental mean values were compared while the avatar in VR moved at different speeds. When the

Preprints (www.preprints.org) | NOT PEER-REVIEWED | Posted: 3 December 2017 doi:10.20944/preprints201712.0012.v1

significance level was less than 0.05, there was a significant difference between the two groups. The results show that there is a significant difference in operating range in the six directions when the virtual object moved at the lowest speed and the highest speed, which indicates that the speed of the virtual object has an effect on the amplitude of the haptic device.

Table 5. LSD multiple comparison results of experimental data of virtual object velocity

Dependent Variable	(I)a	(J)a	Mean Difference (I-J)	Standard Error	significance	95% confidence intervals (CIs)	
						lower limit	upper limit
X+(°)	1.00	2.00	4.17500	2.23082	0.072	-.4023	8.7523
		3.00	6.18800*	2.23082	0.010	1.6107	10.7653
	2.00	1.00	-4.17500	2.23082	0.072	-8.7523	.4023
		3.00	2.01300	2.23082	0.375	-2.5643	6.5903
	3.00	1.00	-6.18800*	2.23082	0.010	-10.7653	-1.6107
		2.00	-2.01300	2.23082	0.375	-6.5903	2.5643
X-(°)	1.00	2.00	-3.68900	3.26252	0.268	-10.3831	3.0051
		3.00	-7.07000*	3.26252	0.039	-13.7641	-.3759
	2.00	1.00	3.68900	3.26252	0.268	-3.0051	10.3831
		3.00	-3.38100	3.26252	0.309	-10.0751	3.3131
	3.00	1.00	7.07000*	3.26252	0.039	.3759	13.7641
		2.00	3.38100	3.26252	.309	-3.3131	10.0751
Y+(°)	1.00	2.00	2.33300	2.48711	.357	-2.7701	7.4361
		3.00	4.98700	2.48711	0.055	-.1161	10.0901
	2.00	1.00	-2.33300	2.48711	0.357	-7.4361	2.7701
		3.00	2.65400	2.48711	0.295	-2.4491	7.7571
	3.00	1.00	-4.98700	2.48711	0.055	-10.0901	.1161
		2.00	-2.65400	2.48711	0.295	-7.7571	2.4491
Y-(°)	1.00	2.00	-5.47200	4.07034	0.190	-13.8236	2.8796
		3.00	-8.28400	4.07034	0.052	-16.6356	.0676
	2.00	1.00	5.47200	4.07034	0.190	-2.8796	13.8236
		3.00	-2.81200	4.07034	0.496	-11.1636	5.5396
	3.00	1.00	8.28400	4.07034	0.052	-.0676	16.6356
		2.00	2.81200	4.07034	0.496	-5.5396	11.1636
Z+(°)	1.00	2.00	10.28330	5.44684	0.070	-.8927	21.4593
		3.00	16.65510*	5.44684	0.005	5.4791	27.8311
	2.00	1.00	-10.28330	5.44684	0.070	-21.4593	.8927
		3.00	6.37180	5.44684	0.252	-4.8042	17.5478
	3.00	1.00	-16.65510*	5.44684	0.005	-27.8311	-5.4791
		2.00	-6.37180	5.44684	0.252	-17.5478	4.8042
Z-(°)	1.00	2.00	-8.10550	7.93309	0.316	-24.3829	8.1719
		3.00	-14.69300	7.93309	0.075	-30.9704	1.5844
	2.00	1.00	8.10550	7.93309	0.316	-8.1719	24.3829
		3.00	-6.58750	7.93309	0.414	-22.8649	9.6899

Preprints (www.preprints.org) | NOT PEER-REVIEWED | Posted: 3 December 2017 doi:10.20944/preprints201712.0012.v1

	3.00	1.00	14.69300	7.93309	0.075	-1.5844	30.9704
		2.00	6.58750	7.93309	0.414	-9.6899	22.8649

Figure 12 shows the histogram of the operating range of the haptic master in the positive and negative directions of X, Y, Z axis under the conditions of three grades of avatar speed. The abscissa in Figure 12 is 1, 2, 3, representing the avatar speed of 0.5cm/s, 1.5cm/s and 2.5cm/s respectively. The vertical axis represents the maximum operating angle in degrees in the corresponding direction.

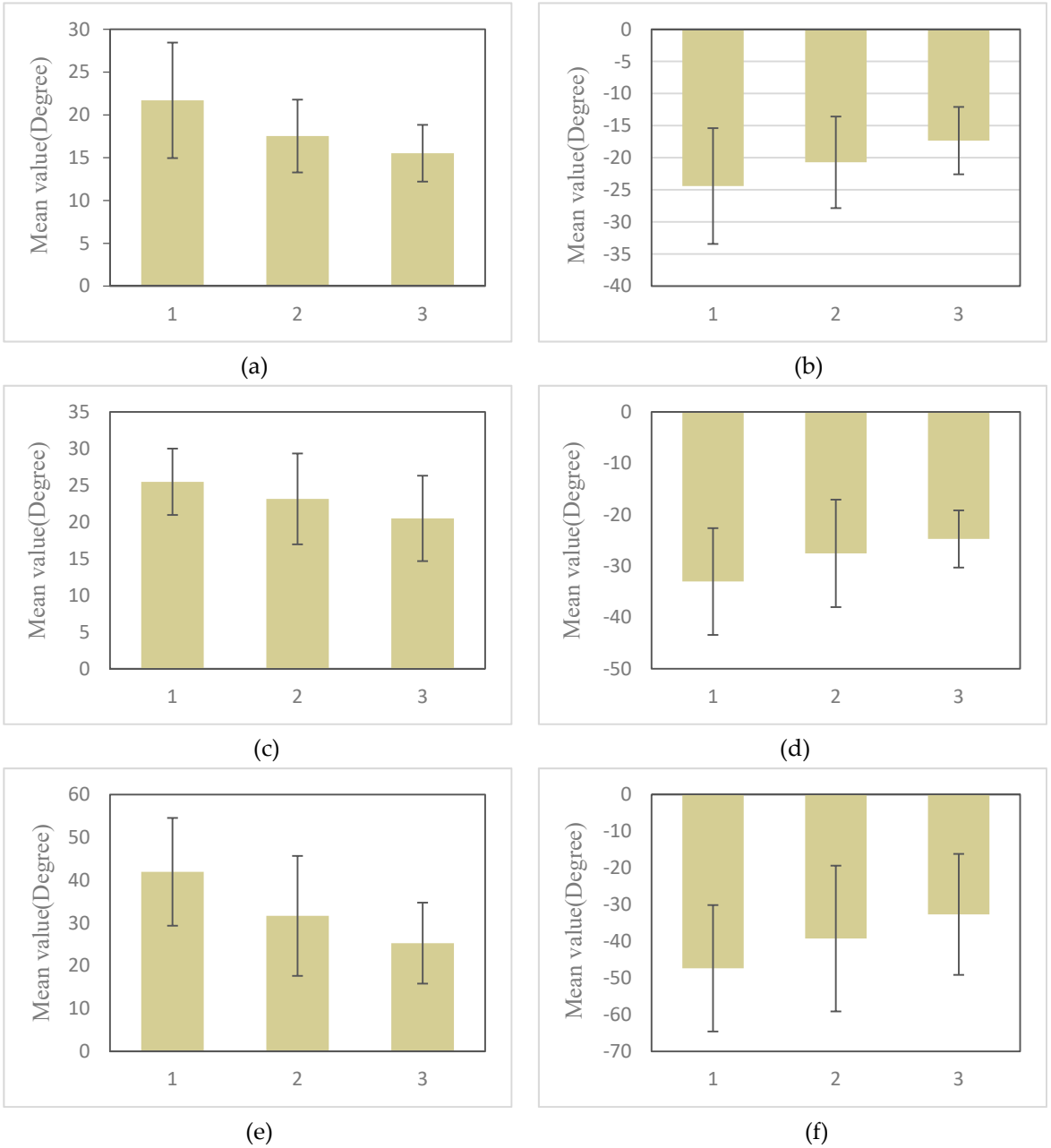

Figure 12. Bar graph of the operating range in six motion directions with three grades of avatar speed. (a)X+; (b)X-; (c)Y+; (d)Y-; (e)Z+; (f)Z-

It can be seen from Figure 12 that of the moving speed of the virtual avatar has a certain influence on the operating range in each direction. The larger the moving speed, the smaller the operating range in the corresponding motion direction.

Preprints (www.preprints.org) | NOT PEER-REVIEWED | Posted: 3 December 2017 doi:10.20944/preprints201712.0012.v1

5.4. Relationship between the Arm Length and the Operating Range

In the experiment, the length of the right arm (the distance from the scapula to the palm) of each subject was measured. Figure 13 shows the scatter plot of the relationship between the operating range and the arm length. The abscissa is the arm length and the ordinate is the average operating range of multiple experiments.

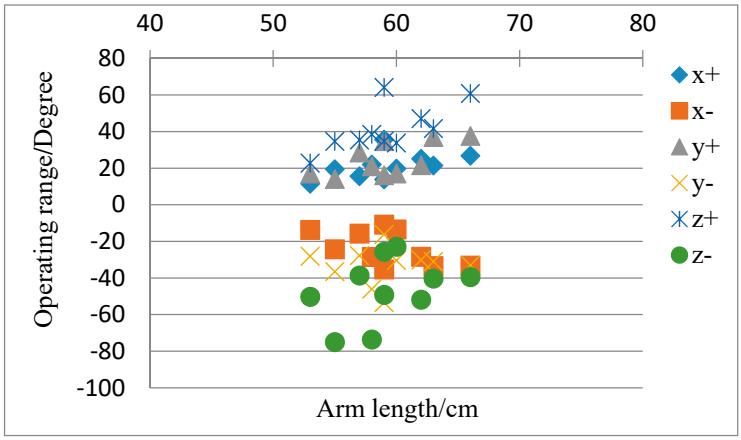

Figure 13. The scatter plot of the relationship between the operating range and the arm length

Method of correlation analysis was applied to study the relevance. In this paper, the spearman correlation coefficient was used to analyze the relationship between the arm length and the operating range. The results are shown in Table 6.

Table 6. Operation space range and arm length correlation coefficient table

			X+ (°)	X-(°)	Y+(°)	Y-(°)	Z+(°)	Z-(°)
Spearman rank correlation coefficient	Arm length (cm)	correlation coefficient	0.638	-0.413	0.675	-0.122	0.626	0.371
		Sig.(double sides)	0.047	0.235	0.032	0.783	0.053	0.291
		N	10	10	10	10	10	10

From the Table 6, the operating range correlates with the arm length in the X-axis Y-axis positive direction at 0.05 significant level. Because the X-axis positive direction is to move the handle of the haptic device to right and the Y-axis positive direction is to move forward, it can be deduced that the operating range and the arm length are positively correlated when the handle is moved away from the body and the correlation coefficients are 0.638 and 0.655 respectively.

5.5. Differences in Operating Range along Different Directions

Table 7 shows the operating ranges of the experimenter in each direction in each experiment, ie, the maximum operating angle.

Table 7. Operating range statistics

		X+(°)	X-(°)	Y+(°)	Y-(°)	Z+(°)	Z-(°)
Speed of virtual object	Slow	21.709	-24.406	25.479	-33.013	41.948	-47.341
	Medium	17.534	-20.717	23.146	-27.541	31.665	-39.235
	Fast	15.521	-17.336	20.492	-24.729	25.293	-32.648
Reset force	Small	22.002	-24.606	25.742	-32.987	43.648	-47.347
	Fast	16.194	-20.453	18.010	-25.108	27.031	-38.595
	Large	15.013	-14.405	16.755	-20.160	27.707	-32.169

Preprints (www.preprints.org) | NOT PEER-REVIEWED | Posted: 3 December 2017 doi:10.20944/preprints201712.0012.v1

As can be seen from Table 7, the maximum range along X and Y negative direction is greater than that along the positive direction. X negative direction represents moving the handle to the left and positive direction represents moving the handle to the right. Similarly, Y negative direction represents moving the handle close to the operator and the positive direction represents moving the handle away from the operator. It can be concluded that the motion of the operator's handle toward himself/herself is greater than moving away from himself/herself. This means that asymmetric control interval is necessary for a haptic-master based system.

5.6. Determination of Operating Range and Operation Speed

Three sets of experiments were taken to study the operating range of the haptic master while the moving speed of the virtual object was controlled at the medium speed, reset force is provided by the rubber bands. According to Table 7 we can obtain that under the above conditions the average range of hand movement is roughly -21.96 ° ~ 19.74 ° along X-axis angle, -29.25 ° to 24.95 ° along Y and -41.60 ° to 39.09 ° around Z axis.

The distance from the end of the handle to the intersection of three axes is about 30cm, so the magnitude of the swing from left to right is about -11.49cm ~ 10.33cm, the magnitude of the swing forwards or backwards is about -15.32cm ~ 13.06cm, and the wrist rotation angle range is -41.60 ° ~ 39.09 °.

In the experiment, the speed at which the operator operates the handle is recorded at the same time, so the maximum operating speed of the operator can be obtained by the above method. Table 8 shows the operating speed of the subjects in each direction in experiments, in degrees per second.

Table 8. Operation speed data statistics

Direction		X+(°/s)	X-(°/s)	Y+(°/s)	Y-(°/s)	Z+(°/s)	Z-(°/s)
Speed of virtual object	Slow	102.333	-111.000	101.999	-103.666	381.943	-347.221
	Medium	83.333	-113.333	76.333	-100.333	280.555	-305.555
	Fast	89.524	-108.095	71.428	-76.666	255.952	-259.920
Reset force	Small	99.333	-101.666	104.332	-101.999	387.499	-348.610
	Fast	98.000	-106.333	90.333	-112.333	255.555	-312.500
	Large	110.000	-110.476	104.761	-89.523	261.904	-287.698

Since the moving speed and the reset force of the virtual avatar have no significant effect on the operating speed, all the experimental results are averaged and the maximum operating speed in different directions can be obtained. The operating speed in X, Y, Z axis is -109.18°/s ~ 98.38°/s, -99.73°/s ~ 92.06°/s, -310.60°/s ~ 300.75°/s respectively. Converted the speed to translation in the workspace, the operating speed from left to right is -57.17cm/s ~ 51.51cm/s, the operating speed forwards and backwards is -52.22cm/s ~ 48.20cm/s. That is, the operators are used to operating the haptic master at such speed and this should be considered while an interactive system is designed using a haptic master.

6. Conclusion

In this study, a novel 3-DOF self-resetting haptic device was designed. The mechanical design avoids coupling between three directions mechanically by using three perpendicular axis intersecting at one point. It can provide three DOF force feedback to human operators. VR-based interactive system using the developed device was built and experiments were conducted. Statistical analysis was used to study the influencing factor including the guiding force, the reset force, the speed of the virtual object and arm length. The experimental results can provide evidence for how to design and optimize the haptic master and the haptic interactive system.

Acknowledgments: This paper is supported by Natural Science Foundation of China under Grants number 61403080 and the National Key Research and Development Program of China (No. 2016YFB1001301).

Author Contributions: Each co-author made important contributions to this research. Huijun Li organized the research. Aiguo Song and Bowei Li joined in the design of the haptic device and conducted calibration experiments. Zhen Lin, Baoguo Xu and Hong Zeng participated in the formulation of main design targets. This writing was finished by Huijun Li and supervised by Aiguo Song. All authors approved the final version of this paper.

Conflicts of Interest: The authors declare no conflict of interest.

References

1. Bolopion A, Régnier S. A review of haptic feedback teleoperation systems for micromanipulation and microassembly[J]. IEEE Transactions on automation science and engineering, 2013, 10(3): 496-502.
2. Sasaki T, Kokubo K, Sakai H. Hydraulically driven joint for a force feedback manipulator[J]. Precision Engineering, 2017, 47: 445-451.
3. Pacchierotti C, Meli L, Chinello F, et al. Cutaneous haptic feedback to ensure the stability of robotic teleoperation systems[J]. The International Journal of Robotics Research, 2015, 34(14): 1773-1787.
4. Oscari F, Oboe R, Daud Albasini O A, et al. Design and Construction of a Bilateral Haptic System for the Remote Assessment of the Stiffness and Range of Motion of the Hand[J]. Sensors, 2016, 16(10): 1633.
5. Laycock S D, Day A M. Recent developments and applications of haptic devices[C], Computer Graphics Forum. Blackwell Publishing, Inc, 2003, 22(2): 117-132..
6. Borro D, Savall J, Amundarain A, et al. A large haptic device for aircraft engine maintainability [J]. IEEE Computer Graphics & Applications, 2004, 24(6):70 - 74.
7. Adams R J, Moreyra M R, Hannaford B. Excalibur, A Three-Axis Force Display[J]. Proc of the Asme Winter Annual Meeting Haptics Symposium, 2010.
8. Çavuşoğlu M C, Feygin D, Tendick F. A critical study of the mechanical and electrical properties of the phantom haptic interface and improvements for highperformance control[J]. Presence: Teleoperators and Virtual Environments, 2002, 11(6): 555-568.
9. Xitact Medical Simulation, http://www.xitact.com
10. Noakes, M., Love, L., and Lloyd, P. 2002. Telerobotic planning and control for DOE D&D operations. IEEE International Conference on Robotics and Automation, Washington DC, pp. 3485–3492.
11. Faulring E L, Colgate J E, Peshkin M A. The cobotic hand controller: design, control and performance of a novel haptic display[J]. The International Journal of Robotics Research, 2006, 25(11): 1099-1119.
12. Bouzit M, Popescu G, Burdea G, et al. The Rutgers Master II-ND force feedback glove[C]. Haptic Interfaces for Virtual Environment and Teleoperator Systems, 2002. HAPTICS 2002. Proceedings. 10th Symposium on. IEEE, 2002:145-152.
13. Schmidt H. HapticWalker-A novel haptic device for walking simulation[C]//Proc. of'EuroHaptics. 2004.
14. He X J, Choi K S. Safety control for impedance haptic interfaces[J]. Multimedia Tools and Applications, 2016, 75(23): 15795-15819.
15. Sun X, Andersson K, Sellgren U, Towards a Methodology for Multidisciplinary Design Optimization, Proceedings of the ASME 2015 International Design Engineering Technical Conferences & Computers and Information in Engineering Conference IDETC/CIE 2015, August 2-5, 2015, Boston, Massachusetts, USA.
16. Qin H, Song A, Liu Y, et al. Design and calibration of a new 6 DOF haptic device[J]. Sensors, 2015, 15(12): 31293-31313.
17. Sauvet B, Laliberte T, Gosselin C. Design, analysis and experimental validation of an ungrounded haptic interface using a piezoelectric actuator[J]. Mechatronics, 2017, 45: 100-109.
18. Sarakoglou I, Garcia-Hernandez N, Tsagarakis N G, et al. A high performance tactile feedback display and its integration in teleoperation[J]. IEEE Transactions on Haptics, 2012, 5(3): 252-263.
19. Sun X, Sellgren U, Andersson K. Situated Design Optimization of Haptic Devices[J]. Procedia CIRP, 2016, 50: 293-298.
20. Tan H Z, Srinivasan M A, Eberman B, et al. Human factors for the design of force-reflecting haptic interfaces[J]. Dynamic Systems and Control, 1994, 55(1): 353-359.

 doi:10.20944/preprints201712.0012.v1

21. Ellis, R.; Ismaeil, O.; Lipsett, M. Design and evaluation of a high-performance haptic interface. Robotica, 1996, 14, 321–327.
22. Yoon W K, Suehiro T, Tsumaki Y, et al. A method for analyzing parallel mechanism stiffness including elastic deformations in the structure[C].Intelligent Robots and Systems, 2002. IEEE/RSJ International Conference on. IEEE, 2002(34):633-634.